Hardening of an ODS Ferritic Steel after Helium Implantation and Thermal Annealing *

Chang-Hao Su(苏长浩)[1,2], Chong-Hong Zhang(张崇宏)[1**], Yi-Tao Yang(杨义涛)[1], Zhao-Nan Ding(丁兆楠)[1], Yu-Guang Chen(陈宇光)[1,2], Akihiko Kimura[3]

[1]*Institute of Modern Physics, Chinese Academy of Sciences, Lanzhou 730000*
[2]*University of Chinese Academy of Sciences, Beijing 100049*
[3]*Institute of Advanced Energy, Kyoto University, Kyoto 611-0011, Japan*

(Received 22 December 2017)

Specimens of an oxide dispersion strengthened (ODS) ferritic steel (15Cr-4Al-0.6Zr-0.1Ti) are implanted with multiple-energy He ions at room temperature to create a damage plateau of 0.4 dpa for the average (corresponding to an He concentration of about 7000 appm) from the near surface to a depth about 1 μm. The specimen is subsequently thermally annealed at 800°C for 1 h in a vacuum so that simple defects can be formed in the as-implanted state that has undergone significant recombination, meanwhile helium bubbles at nano-scale are formed. Hardness of the specimens are tested with the nano-indentation technique. A hardening by 25% is observed. Microstructures of the specimen after irradiation/annealing are investigated with transmission electron microscopy. Helium bubbles are generally located at dislocations and grain boundaries. Using the dispersed barrier strength model, the strength factor of helium bubbles in the ODS ferritic steel is estimated to be between 0.1 and 0.26, which is close to that of helium bubbles in austenitic steels.

PACS: 61.80.−x, 61.82.Bg, 81.40.Cd, 61.72.Ff DOI: 10.1088/0256-307X/35/5/056102

Oxide dispersion strengthened (ODS) ferritic steels are one of the prime candidate structural materials in advanced nuclear reactors, due to their good creep resistance at elevated temperatures, improved resistance to void swelling and reduced activation.[1−4] The response of ODS steels to intensive irradiation of high-energy neutrons, which not only produces the atomic displacement damage but also produces gaseous impurities like helium atoms via (n,α) reaction, is an important concern for the application of the materials in advanced nuclear reactors.[5,6] Irradiated-induced defects (including dislocation loops, voids and bubbles) can cause hardening/embrittlement and thus limit the lifetime of structural components.[7,8] However, how the defects affect the mechanical properties is still unclear, and a thorough understanding is required. The dispersed barrier hardening model is frequently used to describe the relationship between irradiation hardening and microstructure. The strength factors of different kinds of defects have been widely investigated. For example, the strength factors of dislocation loops and voids were reported to be 0.15–0.5[8,9] and 0.6–0.8,[8] respectively. However, there is not a clear result in the case of helium bubbles. Moreover, the heterogeneous distribution of irradiation damage along the depth produced by mono-energy ions, which was frequently used in previous studies, may cause uncertainties in the determination of the strength factors of defects, because the values of hardness tested by nano-indentation are the average of the damaged region. In the present work, the effect of helium bubbles on hardening of ODS steels is investigated. Multiple-energy helium ions are used to produce an irradiation damage plateau below the specimen surface.

Table 1. Chemical compositions of ODS ferritic steel 15Cr-4Al-0.6Zr-0.1Ti.

Composition	C	Si	Mn	P	S	Cr	W	Al	Ti	N	Zr	Y_2O_3	ExO
Content	0.05	0.03	0.04	<0.005	0.002	14.8	1.84	3.7	0.1	0.009	0.63	0.34	0.1

One high-Cr ODS ferritic steel with Ti, Al and Zr addition (15Cr-4Al-0.6Zr-0.1Ti) fabricated in Kyoto University was used in this study. Chemical compositions of the ODS ferritic steel are listed in Table 1. According to previous works, aluminum addition can improve the resistance of corrosion from lead-bismuth eutectic, but coarsens the oxide dispersoids. Zirconium addition results in finer Y-Zr-O oxides and thus helps to retain a high creep strength. The ODS steel was fabricated through procedures of mechanical alloying, canning and degassing followed by hot extrusion at 1150℃ by using argon-gas atomized powder of Fe-C-Cr-Ti mixed with yttria powder (Y_2O_3, with an average diameter of 30 nm). Further thermo-mechanical characteristic treatment was carried out to modify the brittle bamboo-like grains. More details about the process of the fabrication and properties of the ODS ferritic steels were described in Ref. [10].

Disks with a diameter of 3 mm were punched from a 0.3 mm-thick sheet from the steels and were well polished. The normal of the specimen surface is perpendicular to the direction of the hot-extrusion (named as L type). Implantation of helium was performed at the 320 kV high voltage platform in the Institute of Modern Physics (IMP) at Lanzhou. Helium ions of eight successively decreasing kinetic energies of

*Supported by the National Natural Science Foundation of China under Grant No U1532262, and the National Magnetic Confinement Fusion Program of China under Grant No 2011GB108003.
**Corresponding author. Email: c.h.zhang@impcas.ac.cn
© 2018 Chinese Physical Society and IOP Publishing Ltd

500 keV, 400 keV, 300 keV, 200 keV, 120 keV, 60 keV, 30 keV and 15 keV were used to produce a plateau of irradiation damage/helium concentration under the specimen surface. With regard to 500 keV He ions, a fluence of 1×1^{16} He-ion/cm^2 was approached. Fluences of other energies were descended to 0.96, 0.93, 0.88, 0.83, 0.75, 0.56 and 0.33 times the fluence of 500 keV He ions, respectively. Depth profiles of displacement damage and He concentration distribution calculated by SRIM 2013 are shown in Fig. 1 (using the quick calculation mode, with the displacement energy $E_d = 40$ eV).[11] An average displacement damage about 0.4 dpa (displacement per atom) and a He concentration about 7000 appm (atom parts per million) were produced from the near surface to a depth around 1100 nm in the specimens. The specimen temperature was kept at room temperature and the vacuum was kept at 10^{-5} Pa during helium implantation.

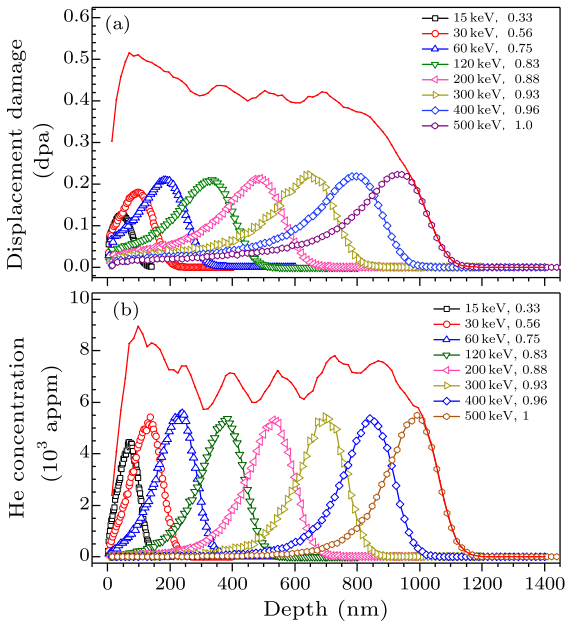

Fig. 1. Depth profiles of (a) displacement damage (dpa) and (b) He concentration (appm) in the ferritic matrix of the ODS steel implanted with He ions with mutiple energy ranging from 500 keV to 15 keV (using quick calculation mode of SRIM2013). The envelope curves are shown in red solid curves.

In general, heliumion implantation in ferritic steels at ambient temperatures produces simple defects, dislocation loops and helium-vacancy clusters in high density (which could result in significant hardening according to our previous study).[12] The subsequent thermal annealing at temperatures above $0.3T_m$ (T_m is the absolute melting point of steels) causes significant recombination of simple defects, rapid growth and coalescence of dislocation loops, and meanwhile causes growth of helium bubbles to the nanometer scale.[13] In the present work, the helium-implanted specimens were subsequently thermally annealed at 800℃ (which is well above $0.3T_m$, meanwhile lower than the temperature for the thermal extrusion for consolidation (1150℃)) for 1 h in a vacuum of 10^{-5} Pa.

To investigate the irradiation hardening, a nanoindentation test was conducted using a nano indenter G200 under the mode of continuous stiffness measurement (CSM)[14,15] at the platform for characterization and test in the Suzhou Institute of Nano-Tech and Nano-Bionics (SINANO). Each specimen was indented at least 9 indents to a depth of 2000 nm. In consideration of the possible consequence of thermal annealing on microstructures, an un-implanted specimen thermally annealed at the same condition (800℃ for 1 h) was tested for comparison.

In addition, microstructures of the specimen were investigated with transmission electron microscopy (TEM). Plan-view TEM samples of the helium-implanted layer were prepared from the helium-implanted and annealed specimens with dimple polishing followed by ion-milling (using a Gatan 690). Thin areas of the samples were investigated in a JEOL 2100F equipped with a LaB_6 electron gun.

Figure 2(a) shows the typical depth distribution of nano-hardness of the ODS ferritic steel with or without helium implantation followed by thermal annealing at 800℃. The curves with error bars show the average of hardness from at least 6 indents on every specimen. From Fig. 2(a), the hardness of the ODS steel after helium implantation and annealing increases, indicating that there is a hardening effect. The indentation size effect (ISE)[16] can be seen in all hardness curves, that is, the nano-hardness decreases with the depth in the region deeper than 100 nm. Data of measured hardness with depth less than 100 nm were not considered because of the reverse ISE and surface artifact.[7]

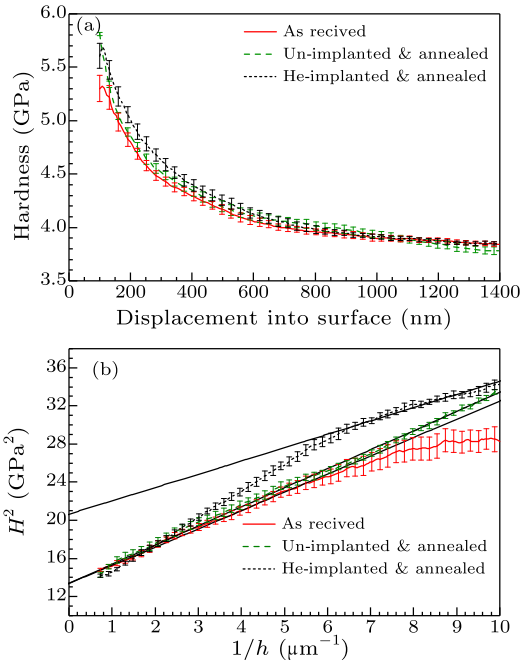

Fig. 2. (a) Indentation-depth dependence of the nano-hardness, and (b) plots of square nano-hardness (H^2) against the reciprocal depth ($1/h$) of 15Cr-4Al-0.6Zr-0.1Ti before and after helium-implantation/annealing.

As far as the ISE is considered, Nix and Gao proposed a model based on the theory of geometrically necessary dislocations to describe the relationship between nano-indentation hardness and depth.[17] The

relationship is given as follows:

$$\frac{H}{H_0} = \sqrt{1 + \frac{h^*}{h}}, \tag{1}$$

$$h^* = \frac{81}{2} b\beta^2 \tan^2\theta \left(\frac{G}{H_0}\right)^2, \tag{2}$$

where H is the measured nano-hardness at the indentation depth h, H_0 is the hardness at infinite depth, i.e., the constitutive nano-hardness, h^* is the characteristic length that depends on the investigation materials and the shape of the indenter tip, β is a constant, b is the Burgers vector, G is the shear modulus, and θ is the angle between the surface of the indenter and the specimen surface.

Considering the convenience of obtaining the constitutive nano-hardness H_0, Eq. (1) is transformed into[18]

$$H^2 = H_0^2\left(1 + \frac{h^*}{h}\right). \tag{3}$$

Based on Eq. (3), the square of measured nano-hardness (H_0) against the reciprocal indentation depth ($1/h$) for the ODS steel is plotted in Fig. 2(b). Theoretically, the square nano-hardness of the un-implanted specimens is proportional to the reciprocal indentation depth with good linearity. The observed deviation from the straight line for the un-implanted specimen without thermal annealing is owing to the effect of deformation in the near surface region caused by the mechanical polishing process. After thermal annealing, the deformation in the un-implanted specimen shows recovery which caused a good linearity as shown in Fig. 2(b). For the helium-implanted specimen, it shows two regimes of linearity, with a clearly distinguished boundary between 140 and 180 nm. The change of the linearity when the indentation depth exceeds the inflection point is attributed to the soft substrate effect (SSE).[19] From Fig. 1, the boundary of the irradiation damage region/un-irradiated region is at a depth of about 1100 nm. In general, the size of the elastically deformed zone is about 5–7 times of the indentation depth,[20] indicating that the elastically deformed zone can reach the undamaged region of the specimens when indented to the depth of 150–220 nm in the present work. According to Eq. (3), the curves are fitted linearly, shown by the black line in Fig. 2(b). The square roots of the intercepts of the fit lines stand for values of the hardness H_0 of the irradiated layers, as listed in Table 2. Obviously, the nano-hardness of the un-implanted specimens before and after thermal annealing are nearly the same, allowing for a certain amount of error. However, in the helium-implanted and thermally annealed specimen, the nano-hardness of the implanted layer is notably higher than the un-implanted specimen.

Table 2. Calculated hardness H_0 and ΔH.

Sample		Hardness (H_0) (GPa)	ΔH (GPa)
15Cr-4Al-0.6Zr-0.1Ti	As received	3.6 ± 0.01	
	Un-implanted & Annealed	3.66 ± 0.02	
	He-implanted & Annealed	4.54 ± 0.09	0.9 ± 0.1

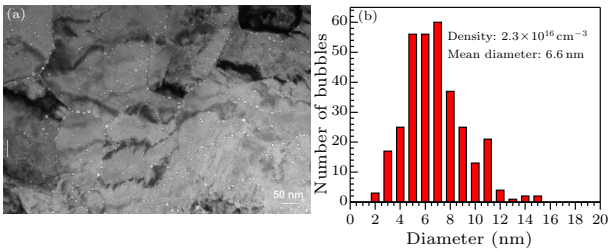

Fig. 3. (a) Bright-field under-focused image of helium bubbles, and (b) the corresponding bubble size distribution.

Figure 3(a) shows a TEM micrograph (in under-focused condition) of the He-implanted region after thermal annealing at 800℃ for 1 h. The image was obtained under a kinematic condition that contrasted from dislocations or precipitates was reduced. Obviously, fine bubbles were formed, preferentially located at grain boundaries. Furthermore, dislocation loops in high-density were not observed in other two-beam conditions in the specimen, indicating that dislocation loops produced by helium implantation at ambient temperature underwent rapid growth, and coalesced with dislocations during the subsequent thermal annealing process at 800℃, as reported in previous works.[21,22] Meanwhile, large voids were not observed in the specimen, indicating that void growth was efficiently suppressed in the ODS steel. It is in agreement with the previous studies on ion-irradiated ODS steels.[23,24] Therefore, this work can focus on the hardening effects from He bubbles which dominate the microstructures after helium-implantation and annealing at 800℃. The histogram of bubble size distribution is shown in Fig. 3(b). The bubbles are ranging from 2 to 15 nm in diameter with the average about 6.6 nm. The number density is about 2.3×10^{16} cm^{-3}, which is determined by measuring the local sample thickness with converged beam electron diffraction technique (CBED).[25] The relative error is estimated to be 20%.

Previous studies show that bubbles can act as obstacles to the dislocation motion, and cause hardening according to the dispersed barrier hardening model[26]

$$\Delta\sigma_{\mathrm{y,b}} = M\alpha G b\sqrt{Nd}, \tag{4}$$

where $\Delta\sigma_{\mathrm{y,b}}$ is the increased value of the yield stress caused by bubbles, M is the Taylor factor, α is the strength factor, N is the number density of the obstacles, d is their average diameter, and b is the Burgers vector. The parameters of M and b are constant for iron-based alloys, taken to be 3.06[27] and 2.5×10^{10},[28] respectively. The shear modules are often regarded to be a constant, taken to be 79 GPa.[29] However, previous study has shown a change of the modules

after irradiation.[30] Elastic modulus obtained by the present nano-indentation test is shown in Fig. 4. The average elastic modulus of specimen after helium implantation and annealing is about 220 GPa. Based on the constitutive relationship of the elastic modulus and the shear modules $G = E/2(1+\mu)$, where μ is Poisson's ratio (0.3 in general), the corrected shear modules can be calculated to be 84.6 GPa.

Based on Eq. (4), the irradiation hardening is described by the change of yield stress $\Delta\sigma_{\rm y}$ in theory. The real change of hardness ΔH is linked to $\Delta\sigma_{\rm y}$ by[31,32]

$$\Delta\sigma_{\rm y} = 3.06\Delta H_{\rm V}, \tag{5}$$

$$HV = 0.76\,H, \tag{6}$$

$$H_{\rm V} = \left(\frac{0.76}{9.8}\right) \times 10^3 \times H, \tag{7}$$

where $H_{\rm V}$ is the Vickers hardness in units of kg/mm^2, and HV is the Vickers hardness expressed in kgf/mm^2. Equation (7) shows the relationship between $H_{\rm V}$ and H, and the latter is expressed in GPa. Assuming that the hardening is caused by helium bubbles only, an estimate of the upper limit of the strength factor α of helium bubbles in ODS ferritic steel is obtained (0.26) according to Eq. (4).

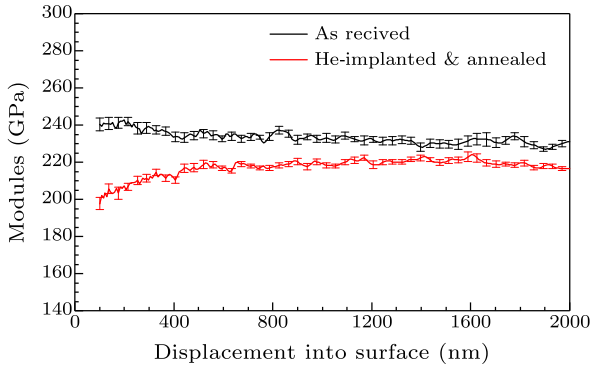

Fig. 4. Indentation-depth dependence of the elastic modulus of the ODS steel before and after helium-implantation/annealing.

Under two-beam image conditions, dislocations in high density can be observed. The density is remarkably higher than that in the un-implanted specimen, indicating that dislocations were built up due to evolution of dislocation loops in the helium-implanted layer during the thermal annealing process. Figure 5 shows a region with the observed highest density of dislocations (about 1×10^{15} m^2). Considering the contribution of dislocation on hardening, the additional increase of the yield stress can be estimated by

$$\Delta\sigma_{\rm y,d} = \lambda G b\sqrt{\rho_{\rm d}}, \tag{8}$$

where $\Delta\sigma_{\rm y,d}$ is the increased value of the yield stress caused by dislocations, $\rho_{\rm d}$ is the dislocation density, and λ is a constant with a reported value of no more than 0.2.[29] Taking account of the contribution of the dislocations (with a density of about 1×10^{15} m^2) to hardening, the lower limit of the strength factor of helium bubbles in the ODS ferritic steel is estimated to be 0.1.

Therefore, the strength factor of helium bubbles in the ODS ferritic steel is estimated to be in the range of 0.1–0.26, which is close to the value of $\alpha \sim 0.2$ for small helium bubbles in austenitic stainless steels as reported by Lucas.[33] Uncertainty of the strength factor of helium bubbles lies in the following aspects. (1) Other defects like dislocation loops may not be eliminated completely by the thermal annealing and may contribute to the observed hardening. (2) Small bubbles with size smaller than 1 nm are not counted because of the resolution limit of TEM. However, the number density of bubbles with size smaller than 1 nm should be much lower than that of the observed bubbles under the present condition, according to the log-normal size distribution of bubbles in steel as proposed by Fell and Murphy.[34] (3) Grain boundaries where helium bubbles preferentially located can block the movement of dislocations, which will weaken the impediment of helium bubbles to dislocation movement. (4) The pinning of dislocation movement by helium bubbles may change with the He atomic density in bubbles, according to the computer simulation work by Yang *et al.*[35] Previous studies show that nanoscale bubbles produced by cold-implantation followed by thermal annealing in pure nickel and steels are in an over-pressurized state (the inner pressure is higher than that of bubbles in equilibrium state).[13] The over-pressurized state of helium bubbles may increase the strength factor to some extent and deserves further investigation.

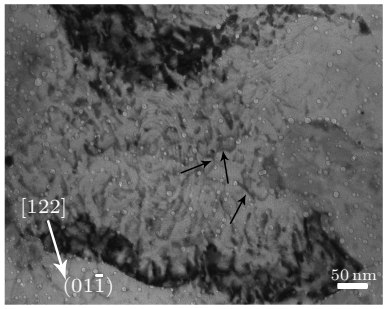

Fig. 5. Image of helium bubbles and dislocations under two-beam condition (g=(011)). The dislocation lines in the grain are marked with arrows in black.

In summary, a hardening of 25% has been produced in the ODS ferritic steel implanted with multiple-energy helium ions to a dose of 0.4 dpa/7000 appm followed by thermal annealing at 800℃ for 1 h. Nano-scale helium bubbles were observed and generally located at dislocations and grain boundaries. Based on the dispersed barrier strength model, the strength factor of helium bubbles in the ODS ferritic steel 15Cr-4Al-0.6Zr-0.1Ti is estimated to be in the range of 0.1–0.26, which is close to that of helium bubbles in austenitic steels.

One of the authors (Chonghong Zhang) thanks the Institute of Advanced Energy, Kyoto University for their supportive visit. We thank the staff of the 320 kV High-voltage Platform in IMP for the help of helium implantation. We also thank Yong Zhang, Lihong Zhou, Tingxing Yan, Liqing Zhang and Yin Song

in IMP and J. S. Lee in Kyoto University for their help in the experiment.

References

[1] Zinkle S J and Busby J T 2009 *Mater. Today* **12** 12
[2] Romanoski G R, Snead L L, Klueh R L and Hoelzer D T 2000 *J. Nucl. Mater.* **283** 642
[3] Yvon P and Carré F 2009 *J. Nucl. Mater.* **385** 217
[4] Ukai S, Nishida T, Okada H and Fujiwara M 1997 *J. Nucl. Sci. Technol.* **34** 256
[5] Mansur L K, Rowcliffe A F, Nanstad R K, Zinkle S J, Corwin W R and Stoller R E 2004 *J. Nucl. Mater.* **329** 166
[6] Yuan D Q, Zheng Y N, Zuo Y, Fan P, Zhou D M, Zhang Q L, Ma X Q, Cui B Q, Chen L H, Jiang W S, Wu Y C, Huang Q Y, Peng L, Cao X Z, Wang B Y, Wei L and Yun S H 2014 *Chin. Phys. Lett.* **31** 046101
[7] Fave L, Pouchon M A, Dobeli M, Borchers M S and Kimura A 2014 *J. Nucl. Mater.* **445** 235
[8] Nakai R, Yabuuchi K, Nogami S and Hasegawa A 2016 *J. Nucl. Mater.* **471** 233
[9] Yabuuchi K, Saito M, Kasada R and Kimura A 2011 *J. Nucl. Mater.* **414** 498
[10] Dou P, Kimura A, Kasada R, Okuda R, Inoue M, Ukai S, Ohnuki S, Fujisawa T and Abe F 2014 *J. Nucl. Mater.* **444** 441
[11] Ziegler J F, Biersack J P and Littmark U 1984 *Stopping Range Ions Solids* (New York: Pergamon) vol 1
[12] Zhang H Q, Zhang C H, Yang Y T, Meng Y C, Jang J and Kimura A 2014 *J. Nucl. Mater.* **455** 349
[13] Singh B N and Trinkaus H 1992 *J. Nucl. Mater.* **186** 153
[14] Li X and Bhushan B 2002 *Mater. Charact.* **48** 11
[15] Zhang Y, Zhang C H, Zhou L H, Li B S and Yang Y T 2010 *Acta Phys. Sin.* **59** 4130 (in Chinese)
[16] Pharr G M, Herbert E G and Gao Y 2010 *Annu. Rev. Mater. Res.* **40** 271
[17] Nix W D and Gao H 1998 *J. Mech. Phys. Solids* **46** 411
[18] Fu Z Y, Liu P P, Wan F R and Zhan Q 2015 *Fusion Eng. Des.* **91** 73
[19] Kiener D 2012 *J. Mater. Res.* **27** 2724
[20] Kasada R, Takayama Y, Yabuuchi K and Kimura A 2011 *Fusion Eng. Des.* **86** 2658
[21] Bhattacharya A, Meslin E, Henry J, Pareige C, Décamps B, Genevois C and Brimbal D 2014 *Acta Mater.* **78** 394
[22] Arakawa K, Hatanaka M, Mori H and Ono K 2004 *J. Nucl. Mater.* **329** 1194
[23] Kim I S, Hunn J D, Hashimoto N and Larson D L 2000 *J. Nucl. Mater.* **280** 264
[24] Zhang C H, Jang J, Cho H D and Yang Y T 2009 *J. Nucl. Mater.* **386** 457
[25] Williams D B and Carter C B 2009 *Transmission Electron Microscopy* (Berlin: Springer) vol 1 chap 20 p 323
[26] Was G S 2007 *Fundamentals of Radiation Materials Science* (Berlin: Springer) chap 12 p 601
[27] Wakai E, Hishinuma A, Usami K, Kato Y, Takaki S and Abiko K 2000 *Mater. Trans.* **41** 1180
[28] Yabuuchi K, Kuribayashi Y, Nogami S, Kasada R and Hasegawa A 2014 *J. Nucl. Mater.* **446** 142
[29] Singh B N, Golubov S I, Trinkaus H, Serra A, Osetsky Y N and Barashev A V 1997 *J. Nucl. Mater.* **251** 107
[30] Odette G R and Frey D 1979 *J. Nucl. Mater.* **85** 817
[31] Yano K H, Swenson M J, Wu Y and Wharry J P 2017 *J. Nucl. Mater.* **483** 107
[32] Busby J T, Hash M C and Was G S 2005 *J. Nucl. Mater.* **336** 267
[33] Lucas G E 1993 *J. Nucl. Mater.* **206** 287
[34] Fell M and Murphhy S M 1990 *J. Nucl. Mater.* **172** 1
[35] Yang L, Zu X T, Gao F and Peng S M 2010 *Physica* B **405** 1754